Intermetallics 111 (2019) 106520

Contents lists available at ScienceDirect

Intermetallics

journal homepage: www.elsevier.com/locate/intermet

Invar effects in FeNiCo medium entropy alloys: From an Invar treasure map to alloy design

Ziyuan Rao[a], Dirk Ponge[a], Fritz Körmann[a,b], Yuji Ikeda[a], Oldřich Schneeweiss[c], Martin Friák[c], Jörg Neugebauer[a], Dierk Raabe[a], Zhiming Li[a,*]

[a] Max-Planck-Institut für Eisenforschung, Max-Planck-Straße 1, 40237, Düsseldorf, Germany
[b] Materials Science and Engineering, Delft University of Technology, 2628 CD, Delft, the Netherlands
[c] Central European Institute of Technology, CEITEC IPM, Institute of Physics of Materials, Czech Academy of Sciences, v.v.i., Žižkova 22, CZ-616 62, Brno, Czech Republic

ARTICLE INFO

Keywords:
Medium entropy alloys
Invar effect
Magnetic properties
Spontaneous volume magnetostriction
Ab initio

ABSTRACT

To facilitate the understanding of Invar effects and design of FeNiCo-base Invar alloys characterized by low thermal expansion coefficient (TEC), we investigated the magnetic and thermal expansion behavior of an equiatomic prototype medium entropy alloy FeNiCo and a non-equiatomic (super Invar) $Fe_{63}Ni_{32}Co_5$ (at. %) reference alloy by means of experiments and *ab initio* calculations. Both alloys consist of a single face-centered cubic phase with fully recrystallized microstructure in the homogenized state. Large spontaneous volume magnetostriction is observed in both alloys below their respective Curie temperatures. The Invar effect in the non-equiatomic $Fe_{63}Ni_{32}Co_5$ alloy is of step-type with nearly zero TEC over a wide temperature range (from room temperature to 120 °C) below its Curie temperature. The equiatomic FeNiCo alloy shows a peak-type Invar effect in a very narrow temperature range (from ~675 °C to ~730 °C) with relatively low TECs. The equiatomic FeNiCo alloy shows both higher saturation magnetization and Curie temperature than the non-equiatomic $Fe_{63}Ni_{32}Co_5$ alloy. The relationships among magnetic behavior, spontaneous volume magnetostriction and Invar effects for a wider array of metallic alloys are discussed mainly based on Masumoto's rule combined with Wohlfarth's itinerant electron theory. An Invar alloy search map is constructed based on the present results and available literature data to visualize the relationships among saturation magnetization, Curie temperature and thermal expansion coefficient for a wide range of Invar alloys. Based on this treasure map a design route for further developments of new Invar alloys by tuning their magnetic properties is discussed.

1. Introduction

The concept of high-entropy alloys (HEAs) containing multiple principal elements was firstly proposed by Yeh et al. [1] and Cantor et al. [2] in 2004. After more than ten years' development, this novel alloy design strategy has added greatly to the field of materials science. Some of specific mechanical and physical properties of HEAs were originally ascribed to entropy maximization [3–5]. However, recent works show that high configurational entropy is not the sole factor for phase stabilization in these materials [6–12]. This finding has motivated researchers to also explore medium-entropy alloys (MEAs) with less principal elements (e.g., 3) and hence lower configurational entropy than suggested by the original HEA concept. Indeed, some recently developed MEAs show outstanding properties comparable to those of equiatomic HEAs. For example, the three-component CoCrNi MEA has been extensively studied recently as it displays strength-toughness combinations exceeding those of most HEAs including the equiatomic CoCrFeMnNi HEA [13–17].

The mechanical properties of many of the currently known HEAs/MEAs have been very carefully investigated [1,3,6,9,13,16,18–22]. Some HEAs/MEAs show excellent mechanical properties at various temperatures due to their multiple strengthening mechanisms, e.g., solid-solution strengthening, precipitation strengthening, twinning- and transformation-induced strengthening [3,9,10,12]. Considering their alloy and manufacturing costs, however, it is still a challenge for HEAs/MEAs to compete with high strength steels, stainless steels, superalloys or Al alloys for demanding cases associated with real structural applications. In this context, it is crucial to explore additional merits of HEAs that may be in reach due to their large accessible compositional spectrum, e.g., undiscovered functional properties. Ideally, joint property profiles that combine high strength and toughness with new functional features are of high interest in this context.

* Corresponding author.
E-mail address: zhiming.li@mpie.de (Z. Li).

https://doi.org/10.1016/j.intermet.2019.106520
Received 14 April 2019; Received in revised form 18 May 2019; Accepted 19 May 2019
Available online 24 May 2019
0966-9795/

Yet, so far only few studies have been devoted to probing broader functional property ranges in this direction. According to the fact that particularly a number of the well-studied HEAs and MEAs contain transition metal elements such as Fe, Ni, Co, Ti, Hf and Zr which are commonly used in magnetic, thermal, shape memory, soft elastic and electrical materials, they have high potential to provide new opportunities for achieving also excellent functional properties, besides their established good mechanical features. For examples, a superconducting HEA made of Ta, Nb, Hf, Zr, and Ti has a critical temperature of 7.3 K [7], and the prototypical Cantor HEA CoCrFeMnNi exhibits very complex low-temperature magnetic properties [23]. Additionally, several kinds of quinary rare-earth HEAs (e.g., GdDyErHoTb) were reported to exhibit the largest refrigerant capacity up to now [8].

Based on these considerations, we suggest that the concept of HEAs/MEAs also provides ample opportunities for exploring new functional features. In this context, one of the most promising directions lies in developing high- or medium-entropy Invar alloys with extremely low thermal expansion in a well-defined temperature range. Established Invar alloys, e.g., $Fe_{64}Ni_{36}$, exhibit a very low thermal expansion coefficient (TEC) below $2 \times 10^{-6} K^{-1}$ around room temperature compared to most metallic materials which have TECs of $10–20 \times 10^{-6} K^{-1}$ [24]. To eliminate or minimize the temperature effect on the dimensions of structural components, these alloys are widely used in precision instruments such as hair springs in watches and also – in huge quantities – in cryogenic applications such as encountered in liquid gas processing and transport. In addition to extremely low TEC, Invar alloys show other anomalous properties, e.g., large spontaneous volume magnetostriction below Curie temperature; large negative pressure effects on magnetization and a large forced-volume magnetostriction. These anomalous properties are called Invar effects. Among these anomalous properties, large spontaneous volume magnetostriction is believed to be the essential character related to the Invar alloys. As a result, another term, i.e., Invar-type alloys, is used to denote the alloys with large spontaneous volume magnetostriction and abnormally lower TEC (not necessarily lower than $2 \times 10^{-6} K^{-1}$) compared to conventional alloys [25–30]. For instance, Fe–Cu alloys prepared by mechanical alloying are not Invar alloys but show an Invar effect, e.g. an abnormal TEC at a temperature range below the Curie temperature [27]. Invar effects have also been found in a variety of other materials including amorphous alloys and intermetallic compounds [25–27,30–36]. After the first discovery of the $Fe_{64}Ni_{36}$ Invar alloy in 1896 [37], new Invar alloys with improved and tailor-made properties have also been developed for specific engineering applications [31,32,34,38–40]. However, Invar alloys are still not fully optimized in terms of several additional features such as strength, toughness, costs, mass density and corrosion resistance. In this context, the concept of HEAs/MEAs provides a great chance for the understanding of Invar effects and further designing of novel Invar alloys.

For this purpose, we investigate in the current study the Invar effects in FeNiCo-base MEAs. The equiatomic FeNiCo alloy is a prototype MEA with maximized configurational entropy. We also study the non-equiatomic $Fe_{63}Ni_{32}Co_5$ MEA, a well-known Invar alloy with a nearly zero TEC around room temperature as reference system. In addition, we performed *ab initio* calculations employing density functional theory to further examine the experimental data. By combining Masumoto's rule which considers saturation magnetization and Curie temperature [41] with Wohlfarth's itinerant electron theory [42–44], we analyzed the effects of magnetic properties which are accessible via *ab initio* calculations (e.g., saturation magnetization and Curie temperature) on the spontaneous volume magnetostriction and Invar effect. Eventually an Invar map is constructed based on our results as well as previous literature data for predicting TEC in alloys for guiding future design of novel Invar MEAs/HEAs.

2. Methodology

2.1. Alloy processing

The ingots of the two alloys, namely $Fe_{63}Ni_{32}Co_5$ and $Fe_{33.4}Ni_{33.3}Co_{33.3}$ (all in at. %) with the same dimensions of $25 \times 60 \times 65\,mm^3$ were cast in a vacuum induction furnace using cleaned metals (> 99.8% purity). Samples with dimensions of $25 \times 60 \times 10\,mm^3$, machined from the original cast, were subsequently hot-rolled at 900 °C to a thickness reduction ratio of 50% (thickness changed from 10 to 5 mm). After hot-rolling, the samples were homogenized at 1200 °C for 2 h in Ar atmosphere followed by water-quenching. The exact composition of the homogenized alloys was obtained by chemical analysis and the results are listed in Table 1.

2.2. Microstructural characterization

The microstructures of the homogenized alloys were analyzed using multiple probing methods. X-ray diffraction (XRD) measurements were performed using an X-Ray equipment ISODEBYEFLEX 3003 equipped with Co $K\alpha_1$ ($\lambda = 1.788965$ Å) radiation operated at 40 kV and 30 mA. Electron backscatter diffraction (EBSD) measurements were carried out by a Zeiss-Crossbeam XB 1540 FIB scanning electron microscope (SEM) with a Hikari camera and the TSL OIM data collection software. Back-scattered electron imaging (BSEI) was performed on a Zeiss-Merlin instrument. The grain sizes in the homogenized alloys were calculated from multiple BSE images and EBSD maps by the intercept method. The elemental distributions in the homogenized alloys were investigated using energy-dispersive X-ray spectroscopy (EDS) at microscale. Prior to the microstructural analysis, fine polishing of the samples' surfaces was conducted using an oxide suspension (OPS) with silica particle sizes around 50 nm for more than 30 min to effectively remove the deformation layer caused by mechanical grinding. The sample surfaces were finally polished with soap and ethanol for 5 min to remove the nano-silica particles.

2.3. Magnetic and thermal property measurements

Temperature dependences of magnetic moments of the two MEAs were measured using a VSM magnetometer (EG&G PARC) with an electromagnet (1.5 T) in an external field 10 mT over a temperature range of 25–800 °C in vacuum. Hysteresis loops were taken at room temperature in an external magnetic field of ± 1 T before measurements of the temperature dependence of the magnetic moment. The thermal expansion behavior was measured in a thermal dilatometer from room temperature to 950 °C at a heating rate of 2 °C/min in argon atmosphere. Hollow cylindrical tube samples of the MEAs with length of 9 mm, outer diameter of 4 mm and wall thickness of 1 mm were prepared for the thermal expansion tests. We use hollow samples because they exhibit more uniform temperature distribution upon heating and cooling compared to solid samples.

2.4. Density functional theory calculations

Density functional theory calculations were performed employing the exact-muffin-tin-orbital (EMTO) method [45] in combination with

Table 1
Compositions of the homogenized equiatomic FeNiCo and non-equiatomic $Fe_{63}Ni_{32}Co_5$ MEAs measured by wet-chemical analysis (at. %).

Alloys	Fe	Ni	Co
$Fe_{33.4}Ni_{33.3}Co_{33.3}$	33.1	33.4	33.5
$Fe_{63}Ni_{32}Co_5$	62.8	32.2	5.0

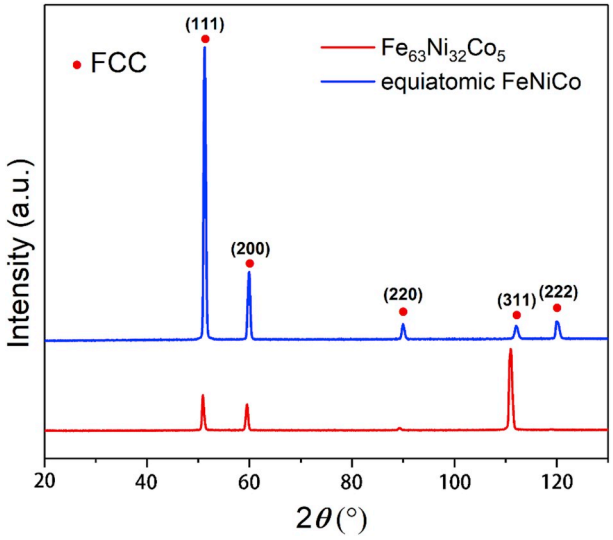

Fig. 1. XRD patterns of the homogenized equiatomic FeNiCo and non-equiatomic $Fe_{63}Ni_{32}Co_5$ MEAs. Both alloys show single FCC phase.

the full-charge-density (FCD) method [46,47]. The substitutional disorder was modeled using the coherent potential approximation [48,49]. The DFT energies were calculated within the generalized-gradient approximation (GGA) [50]. A 40 × 40 × 40 *k*-point mesh per unit cell has been chosen. The spontaneous volume magnetostriction has been computed by deriving the ferromagnetic and paramagnetic equation of state and comparing the resulting equilibrium volumes. The paramagnetic state has been simulated by employing the disordered local moment approach based on the EMTO-CPA formalism [51–53], where EMTO-CPA stands for 'exact muffin-tin orbitals theory within the coherent potential approximation'. The energy difference between both magnetic states is used to derive the Curie temperature based on the mean field approximation [54]. For a comprehensive review of *ab initio* calculations for HEAs and MEAs we refer to Ref. [55].

3. Results

3.1. Microstructure and compositional homogeneity

Fig. 1 shows the XRD patterns of the equiatomic FeNiCo and non-equiatomic $Fe_{63}Ni_{32}Co_5$ MEAs. Both alloys have a single-phase face-centered cubic (FCC) structure in the homogenized state. The lattice parameters of the equiatomic FeNiCo and non-equiatomic $Fe_{63}Ni_{32}Co_5$ alloys are 0.35963 and 0.36056 nm, respectively, being in fair agreement with the computed lattice parameters of 0.35596 and 0.35925 nm. EBSD maps presented in Fig. 2a_1 and 2b_1 confirm the single FCC structure of the two alloys. Both alloys are fully recrystallized with a high number density of annealing twins. According to the calculation from multiple BSE images and EBSD maps, the average grain sizes of non-equiatomic $Fe_{63}Ni_{32}Co_5$ and equiatomic FeNiCo are ~56 μm and ~45 μm (excluding annealing twin boundaries), respectively. Fig. 2$a_{2\text{-}5}$ and 2$b_{2\text{-}5}$ show the BSE images and EDS maps of the non-equiatomic $Fe_{63}Ni_{32}Co_5$ and equiatomic FeNiCo alloys, suggesting that all the elements (Fe, Co and Ni) are uniformly distributed in the microstructure. This observation further suggests that the effects of elemental segregation on the magnetic and thermal behavior can be excluded in the current non-equiatomic $Fe_{63}Ni_{32}Co_5$ and equiatomic FeNiCo MEAs.

3.2. Magnetic properties

Fig. 3 presents the magnetic behavior of the equiatomic FeNiCo and non-equiatomic $Fe_{63}Ni_{32}Co_5$ MEAs. Fig. 3a shows the demagnetization behavior of the two alloys as a function of temperature at a magnetic field strength of 1 mT. The Curie temperature of the equiatomic FeNiCo alloy is about 720 °C while that of the $Fe_{63}Ni_{32}Co_5$ alloy is only about 260 °C. Considering that the Curie temperatures of Fe, Ni and Co are about 770, 354 and 1127 °C, respectively, plain linear interpolation suggests that the higher content of Co in the equiatomic FeNiCo alloy system might also lead to a higher Curie temperature. This is also in agreement with our DFT calculations which predict a Curie temperature of 595 °C and 261 °C for equiatomic FeCoNi and $Fe_{63}Ni_{32}Co_5$, respectively. The result for FeCoNi is also in agreement with previous calculations [56] and somewhat below the experimental value observed in the current study (720 °C, Fig. 3a). We note the underestimation of the Curie temperature for FeCoNi. A similar underestimated Curie temperature is obtained for pure Ni [57], which could be improved in future by including thermally induced longitudinal spin fluctuations in the computational scheme based on the approach developed, e.g., in Ref. [57].

According to the hysteresis loops in Fig. 3b, both the equiatomic FeNiCo and non-equiatomic $Fe_{63}Ni_{32}Co_5$ alloys exhibit typical features of soft magnetic materials with high saturation magnetization and low coercivity. The saturation magnetization of the equiatomic FeNiCo alloy is about 160 emu/g while for the $Fe_{63}Ni_{32}Co_5$ alloy it is around 145 emu/g. The values are in fair agreement with the simulated data of 158 emu/g for FeNiCo and 160 emu/g for $Fe_{63}Ni_{32}Co_5$. The overestimated saturation magnetization of the $Fe_{63}Ni_{32}Co_5$ alloy might be related to potential antiferromagnetic configurations (not included in the present calculations) as discussed for $Fe_{64}Ni_{36}$ in Ref. [57]. The saturation magnetization of alloys can be also roughly approximated by using Vegard's linear mixing rule from the product of the net magnetic moment for each atom in its stable phase [58]. Here the net magnetic moments per atom for Fe, Co, and Ni are 2.22, 1.72, and 0.60 Bohr magnetons (μ_B), respectively [58,59]. As a result, the saturation magnetization for 3d-transition metals and alloys changes as a function of the number of electrons per atom. As shown in Fig. 4, most alloys such as binary Ni–Co, Co–Fe and Fe–Ni follow the Slater-Pauling curve [24,58,60] which approximates the maximum magnetic moment of transition metals and their alloys. From Fig. 4, the relationship between the number of electrons per atom and the saturation magnetic moment per atom for the equiatomic FeNiCo MEA fits onto the Slater-Pauling curve, while that for the $Fe_{63}Ni_{32}Co_5$ alloy deviates from it. This observation suggests that $Fe_{63}Ni_{32}Co_5$ alloy is ferromagnetically unstable and the saturation magnetization is below the value predicted by the Slater-Pauling curve. Also, the Fe, Ni and Co atoms do not possess full magnetic moments in the $Fe_{63}Ni_{32}Co_5$ alloy. Similar features have also been found in other Invar alloys such as the $Fe_{64}Ni_{36}$ reference material. This could be due to antiferromagnetic configurations as discussed in Ref. [57].

3.3. Thermal expansion behavior

Fig. 5a shows the change in length of the equiatomic FeNiCo and $Fe_{63}Ni_{32}Co_5$ alloys as a function of temperature. When the temperature is below the Curie temperature, the slopes of the thermal expansion curves for both alloys are much smaller as compared to their high temperature state, i.e. for ranges above the Curie temperature. This phenomenon is essentially characterized by large values of spontaneous volume magnetostriction, ω_s, which is defined as a fractional volume change caused by spontaneous magnetization and calculated as

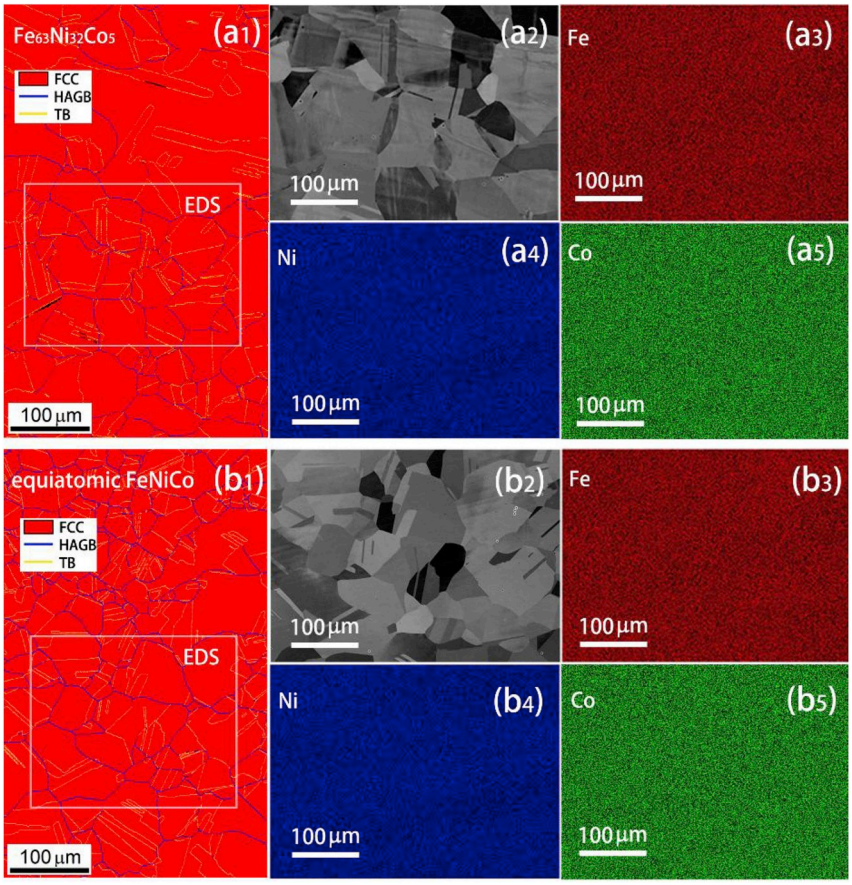

Fig. 2. Microstructure and elemental distribution of ($a_{1\text{-}5}$) equiatomic FeNiCo and ($b_{1\text{-}5}$) non-equiatomic $Fe_{63}Ni_{32}Co_5$ MEAs in homogenized state. (a_1), (b_1) EBSD phase and boundary maps; (a_2), (b_2) BSE images; ($a_{3\text{-}5}$, $b_{3\text{-}5}$) EDS maps of the constituent elements Fe, Ni and Co with an identical sample region in (a_2) and (b_2), respectively.

$\omega_s \approx 3\Delta(dL/L_0)$, where L is the sample length, L_0 is the sample length at a reference temperature, e.g., at room temperature. The spontaneous volume magnetostriction ω_s at room temperature can be obtained by linear extrapolation of the dL/L_0 vs T curves to room temperature. Accordingly, the ω_s values for the two alloys are indicated in Fig. 5a, suggesting that the $Fe_{63}Ni_{32}Co_5$ reference alloy has a larger ω_s value than the equiatomic FeNiCo MEA. This is consistent with our DFT simulation results where the spontaneous volume magnetostriction at 0 K is found as 2.6% for FeCoNi and 4.1% for $Fe_{63}Ni_{32}Co_5$. The latter value is larger than the one for a similar alloy reported in Ref. [57] where a similar DFT approach was applied to a $Fe_{64}Ni_{36}$ Invar alloy, yielding a magnetostriction value of 3%. Our results hence suggest a weakened/enhanced Invar behavior for FeCoNi/$Fe_{63}Ni_{32}Co_5$ as compared to $Fe_{64}Ni_{36}$.

Fig. 5b shows the thermal expansion coefficient (TEC) of the two alloys as a function of temperature. The TEC (α) was calculated by the following equation:

$$\alpha = \frac{d}{dT}\left(\frac{L}{L_0}\right) \quad (1)$$

where L is the sample length, T is the temperature, L_0 is the sample length at room temperature. The equiatomic FeNiCo and non-

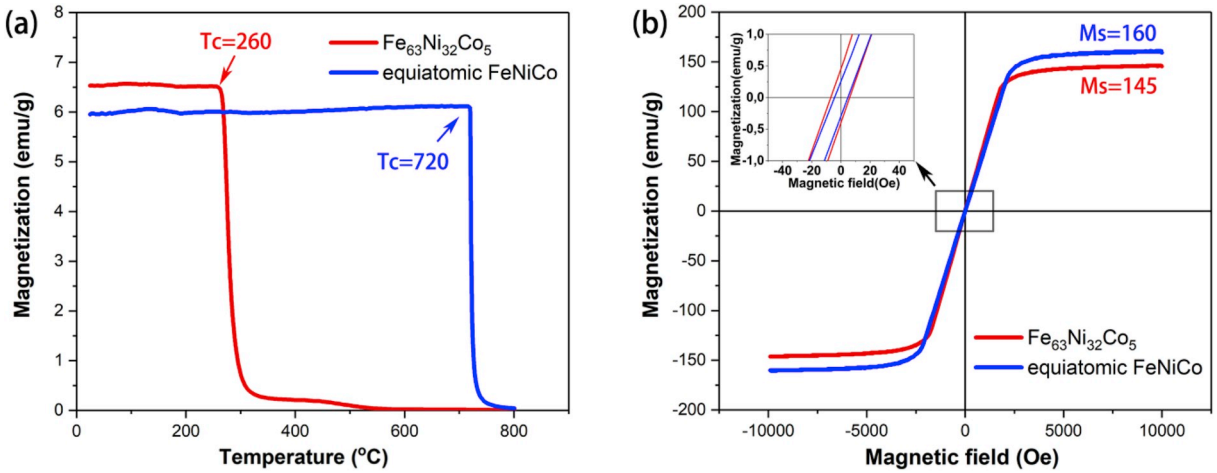

Fig. 3. Magnetization of the homogenized equiatomic FeNiCo and $Fe_{63}Ni_{32}Co_5$ alloys. (a) demagnetization behavior as a function of temperature from 25 to 800 °C at 10 mT in vacuum; (b) hysteresis loops investigated up to 1 T at room temperature. The magnetization is plotted as magnetic moment in units of emu/g, where emu stands for electromagnetic unit. It translates to 1 erg/G, 10^{-3} A m^2 or 10^{-3} J/T.

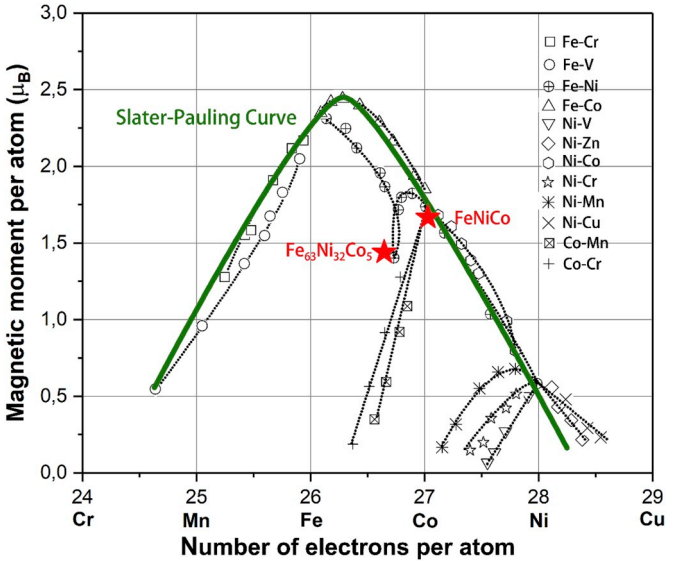

Fig. 4. Saturation magnetic moment (M_s) per atom vs. the number of electrons per atom of the transition metals and alloys compared with $Fe_{63}Ni_{32}Co_5$ and equiatomic FeNiCo. The $Fe_{63}Ni_{32}Co_5$ reference alloy deviates from the Slater-Pauling curve in contrast to the equiatomic FeNiCo MEA. The green solid curve shows the so called Slater-Pauling curve. The black dotted curves and the individual symbols represent the experimental data for 3d-transition metals and alloys from the literature [59,61].

equiatomic $Fe_{63}Ni_{32}Co_5$ alloys show different types of Invar effects: for $Fe_{63}Ni_{32}Co_5$, a step-type Invar effect occurs which indicates that a low TEC exists over a wide temperature range below the Curie temperature; for equiatomic FeNiCo, a peak-type Invar effect is observed which means that the low TEC temperature range is quite narrow compared to the reference material [29]. Fig. 5a shows that the TEC of the $Fe_{63}Ni_{32}Co_5$ alloy drops to near-zero below the Curie temperature, which is much lower than that of the equiatomic FeNiCo alloy. The equiatomic FeNiCo shows its lowest TEC of 7×10^{-6} K near the Curie temperature. Interestingly, when heated above the Curie temperature, both alloys show very similar TEC values. The similar TEC value ($\sim 19 \times 10^{-6}$ K) indicates that in the paramagnetic regime, where no magnetostriction effects are present, the composition changes do not significantly affect the thermal expansion of FeNiCo-base MEAs.

4. Discussion

Since the first discovery of the Invar alloy in 1896 [37], investigations on these materials and the related effects have continued [31,32,34,38–40]. On the one hand, experimental and theoretic studies have been conducted to reveal the mechanism responsible for the Invar anomaly, and several theories have been proposed [24,62] though the origin of the Invar effect is still under debate and unsolved. In recent decades, *ab initio* calculations have also been used to address the Invar effect [57,63–66]. For example, a competition between a low-spin (LS) and a high-spin (HS) state in Fe–Ni alloys was analyzed not only in the bulk state [67] but also in thin Fe–Ni films [68]. Ferromagnetic-to-non-collinear transitions in Fe–Ni alloys were analyzed using theoretical methods in connection with the Invar effect in Ref. [69]. A response of the Fe–Ni alloys to pressure was studied by combining experiments and quantum-mechanical calculations in Ref. [70]. Inter-atomic bond-length distortions were examined by *ab initio* methods in Ref. [71] and Mössbauer spectroscopy and first-principles calculations were used to analyze relations between local magnetic moments of atoms and their environment in Ref. [72].

Alternative materials design approaches lie in using data-driven methods, which are based on identifying suitable descriptors that correlate with the Invar effect. One example for this are, e.g., compositional maps such as used before for phase change materials. These maps are spanned by different atom-property related quantities such as the degree of iconicity [73]. Such descriptors, even if they correlate with the target materials property, do not necessarily describe the underlying physical mechanisms directly, but provide a correlation-based approach for identifying promising candidate materials. A key motivation for the present study has been to identify and evaluate such materials descriptors correlating with the Invar anomaly and not to improve or advance existing methodological approaches and theories.

Despite the recent advances concerned with the computational modelling of the Invar effect for selected alloys, full-field *ab initio* techniques are computationally too expensive for screening a large number of alloys let alone the complex chemical compositional phase space inherent of HEAs. In the present work we thus follow an alternative strategy by finding and evaluating straightforward parameters accessible from simulations such as the ground-state magnetization, a quantity which has been tested in former works for common Invar alloys. One of the aims of the present study is to combine the previous experimental data in this respect and evaluate the magnetization as a potential descriptor for the screening of Invar multicomponent alloys.

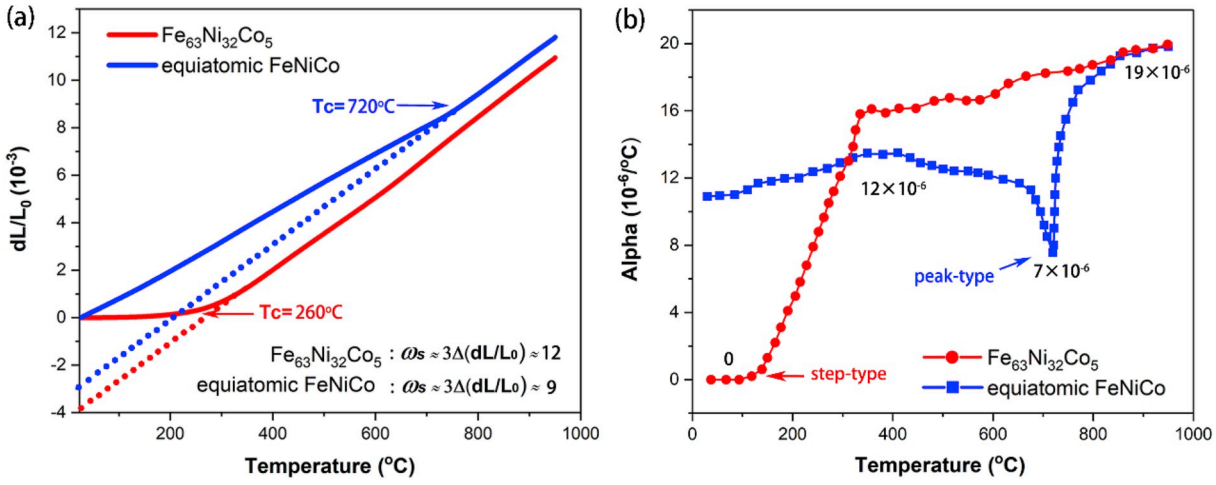

Fig. 5. Thermal expansion behavior of the homogenized equiatomic FeNiCo and non-equiatomic $Fe_{63}Ni_{32}Co_5$ alloys. (a) Change in length as a function of temperature; (b) Thermal expansion coefficient α as a function of temperature. The spontaneous volume magnetostriction ω_s in (a) is at room temperature. The heating rate is 2 °C/min.

In this respect we have resorted to semi-empirical models such as the Masumoto's model, which turned out to be efficient. The Wohlfarth theory, being of similar practical form, has been also evaluated for test purposes. As also shown in this study, many important parameters (e.g., spontaneous volume magnetostriction and Curie temperature) for assessing the Invar behavior can be modeled by full-field *ab initio* calculations. Yet, at a more phenomenological scale Masumoto's model has turned out as a very practical method for identifying Invar alloys by using certain correlations. Its use has led to the discovery of a stainless Invar alloy [33], and has also been pertinent for finding amorphous and intermetallic compound Invar alloys [24–26]. The following discussion is mainly based on Masumoto's model, and an Invar map is constructed to guide corresponding alloy design directions.

4.1. Relationship between magnetic behavior and spontaneous volume magnetostriction

The literature review shows that the relationship between the magnetic properties and spontaneous volume magnetostriction has been extensively discussed for conventional metals and alloys. In the present study, we therefore focus on three-component FeCoNi-base MEAs and compare them to conventional materials. In an early study of Invar effects in Fe–Ni binary alloys by Masumoto [41], it was proposed that the ferromagnetic expansion, here referred to as spontaneous volume magnetostriction ω_s, is proportional to the saturation magnetization M_s at room temperature for FCC solid solutions of varying compositions according to the relation

$$\omega_s = k\, M_s \tag{2}$$

where k is a constant depending on the different alloy systems. Afterwards, Wohlfarth suggested that the FCC structured $Fe_{100-x}Ni_x$ (x = 25–50 at. %) Invar alloys belong to the class of weak itinerant ferromagnets [43,44]. Based on this observation a number of properties, including the large spontaneous volume magnetostriction of Invar alloys, could be qualitatively related to the itinerant electron model of magnetism [43]. As a result a quadratic dependence of the spontaneous volume magnetostriction has been proposed, i.e.

$$\omega_s = A\, M_s^2 \tag{3}$$

where A is a constant related to the magneto-elastic coupling constant [43]. This relation has been confirmed to be valid in Fe–Pt Invar alloys and visualized when plotting ω_s against M_s^2 [74].

Equation (2) proposed by Masumoto and equation (3) proposed by Wohlfarth have been validated for different alloy systems as mentioned above. Both models suggest that a higher saturation magnetization should induce a larger spontaneous volume magnetostriction in an alloy system. However, equiatomic FeNiCo has a lower saturation magnetization and a larger spontaneous volume magnetostriction as compared to $Fe_{63}Ni_{32}Co_5$. In order to understand this phenomenon we first discuss Masumoto's M_s-ω_s relationship for the case of Fe–Ni binary alloys which are compositionally close to the FeNiCo-base MEA systems studied here [41]. Fig. 6 shows that two types of relationships between M_s and ω_s can be revealed for the case of Fe–Ni binary alloys. The first one, marked in green, applies for alloys ranging from $Fe_{70}Ni_{30}$ to $Fe_{60}Ni_{40}$, following the linear relationship $y = 0.029\,x$, and the second one, marked in blue, presents alloys ranging from $Fe_{60}Ni_{40}$ to pure Ni fitting the quadratic relationship $y = 0.00016x^2 + 0.92$. It is well-established that with the increase of Ni, alloys from the composition range $Fe_{70}Ni_{30}$ to $Fe_{60}Ni_{40}$ deviate from the Slater-Pauling curve whereas alloys ranging from $Fe_{50}Ni_{50}$ to pure Ni follow it as shown in Fig. 4. This interesting phenomenological correlation reveals that Fe–Ni binaries can be separated into two classes which follow different rules, namely, the "Slater-Pauling deviation alloys" and the "Slater-Pauling alloys". The "Slater-Pauling deviation alloys", ranging from $Fe_{70}Ni_{30}$ to $Fe_{60}Ni_{40}$, follow Masumoto's rule as given in equation (2). The "Slater-Pauling alloys",

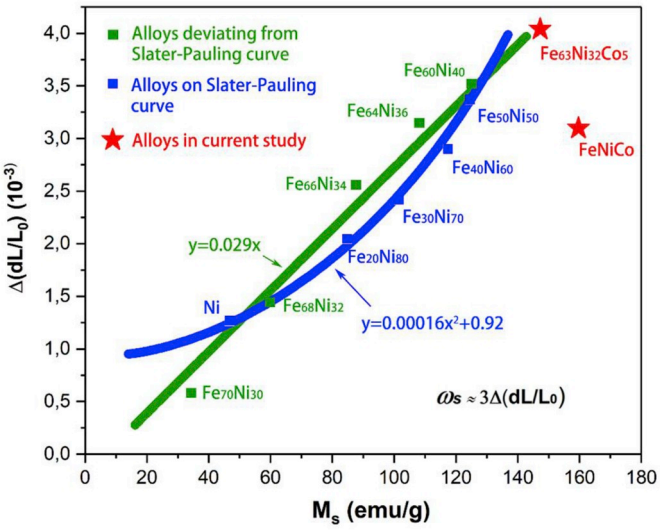

Fig. 6. Relations between $1/3\omega_s$ and M_s in the equiatomic FeNiCo and the non-equiatomic $Fe_{63}Ni_{32}Co_5$ alloys compared to the FCC structured Fe–Ni binary alloys, where ω_s is the spontaneous volume magnetostriction and M_s is the saturation magnetization. The data for the Fe–Ni binary alloys are taken from Masumoto's work for room temperature [41]. Alloys in green color deviate from the Slater-Pauling curve (see Fig. 4) and their $1/3\omega_s$ vs M_s relationship follows a linear rule. Alloys in blue color follow the Slater-Pauling curve and their $1/3\omega_s$ vs M_s relationship fits the quadratic law, following Wohlfarth's model.

ranging from $Fe_{60}Ni_{40}$ to pure Ni follow Wohlfarth's model as given in equation (3). In the present study the non-equiatomic $Fe_{63}Ni_{32}Co_5$ alloy deviates from the Slater-Pauling curve while the equiatomic FeNiCo alloy is on the curve (see Fig. 6). This difference suggests that the relationship between M_s and ω_s existing in both alloys does not solely follow equation (2) or equation (3). The non-equiatomic $Fe_{63}Ni_{32}Co_5$ alloy behaves consistent with equation (2) while the equiatomic FeNiCo alloy reveals closer agreement with equation (3). We note that the equiatomic FeNiCo alloy deviates particularly strong from those alloys that follow the Slater-Pauling curve as shown in Fig. 6 (indicated by the blue line). This can most likely be ascribed to a different constant A in equation (3) for the equiatomic FeNiCo-base MEA, caused by different magneto-elastic coupling effects compared to the FeNi binary alloys.

4.2. Relationship between magnetic properties and invar effect

Magneto-volumetric effects are general features of ferromagnetic alloys [24]. Since the Invar effect is generally limited to temperatures below the Curie temperature, it is reasonable to ascribe this abnormal phenomenon to large spontaneous volume magnetostriction. Ferromagnetic Invar alloys can in general be classified into three types: Fe-rich classical Invar alloys, ferromagnetic amorphous Invar alloys and ferromagnetic intermetallic Invar compounds. In the present study, we focus on revealing the relationship between the magnetic properties and the thermal expansion behavior. Antiferromagnetic Invar alloys are not included in the present considerations. It is well-established that all ferromagnetic Invar alloys show large spontaneous volume magnetostriction ω_s compared with other alloys. For instance, at room temperature, the ω_s of the $Fe_{64}Ni_{36}$ Invar alloy is $\sim 9 \times 10^{-3}$ compared to that of pure Ni which is only $\sim 4 \times 10^{-3}$ [41]. In the present study, the equiatomic FeNiCo and the non-equiatomic $Fe_{63}Ni_{32}Co_5$ alloys show large values for ω_s of $\sim 12 \times 10^{-3}$ and $\sim 9 \times 10^{-3}$, respectively. The $Fe_{63}Ni_{32}Co_5$ alloy exhibits a smaller TEC than the classical $Fe_{64}Ni_{36}$ Invar alloy, but the equiatomic FeNiCo only shows a low TEC of $\sim 7 \times 10^{-6}\,K^{-1}$ in the vicinity of T_c. This observation suggests that a large spontaneous volume magnetostriction alone does not lead to a low thermal expansion coefficient. As discussed below the Curie

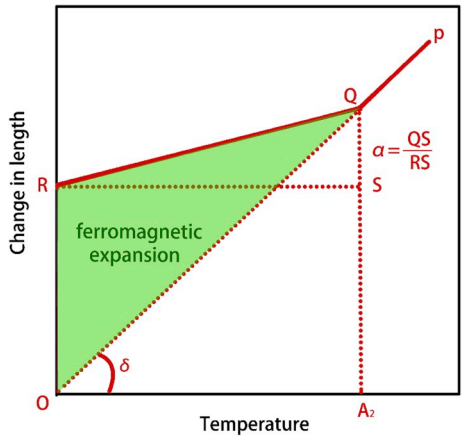

Fig. 7. The schematic model of Masumoto's theory for describing the relationship among thermal expansion coefficient, spontaneous volume magnetostriction and Curie temperature. The green area indicates the ferromagnetic expansion described by Masumoto's relation [41]. The points O and A_2 represent room temperature and Curie temperature, respectively. The line RQ and QP represent the change in length below and above Curie temperature. The length of the line OR presents the spontaneous volume magnetostriction at room temperature.

temperature also plays an important role for the TEC of these ferromagnetic alloys.

As mentioned above Masumoto proposed an empirical rule regarding the Invar effect in alloys, describing that "the circumstances whether a ferromagnetic alloys may have small expansion depend merely on the ratio of the saturation magnetization to the transformation (i.e. the Curie) temperature and the greater the ratio, the smaller the coefficient of expansion becomes" [41]. Following this rule, novel Invar alloys have been found in different systems. For instance, the value of M_s/T_c reaches a maximum value at a Mn concentration of 23.85% in the Co–Mn binary alloy system, and a minimum TEC also appears for the same composition [75]. In another example, the TEC of the Fe–B amorphous alloys becomes smaller with the decrease of the B content since that the Curie temperature decreases remarkably while the saturation magnetization slowly increases which lead to a larger value of M_s/T_c [25]. In the present study, we discuss the relationship between two magnetic features, viz. the magnetic saturation which is a measure for the maximum attainable magnetic moment and the spontaneous volume magnetostriction on the one hand and the thermal expansion coefficient on the other hand, based on Masumoto's theory as used for Fe–Ni binary alloy system (see Fig. 7). As sketched in Fig. 7, in a simplified picture, the expansion linearly increases with increasing temperature up to the Curie temperature (A_2). Above this temperature, the TEC changes abruptly and shows much higher values than below the Curie temperature. The alloys show a smaller TEC in the ferromagnetic state than in the paramagnetic state. If we plot a line PQ down to room temperature (O), the ordinate OR represents the expansion caused by the ferromagnetic state of the alloys. This can be denoted as "ferromagnetic expansion" which is connected to the spontaneous volume magnetostriction. In Masumoto's model, the TEC is determined by the ratio of QS/RS. This suggests that if the QS/RS ratio is smaller, the alloy will have a smaller TEC near room temperature, i.e. in the ferromagnetic state. To simplify this further, the slope δ of the line OQ is approximated as constant resulting in a constant TEC in the paramagnetic state. Based on these considerations the TEC in the ferromagnetic state can be calculated as

$$\alpha = \frac{QS}{RS} = \frac{QA_2 - SA_2}{T_c} = \frac{QA_2}{T_c} - \frac{SA_2}{T_c} = \tan\delta - \frac{\frac{1}{3}\omega_s}{T_c} \quad (4)$$

If we ignore changes of tan δ, which indicates the TEC of alloys in the paramagnetic state, the low TEC is thus solely determined by the ratio of ω_s/T_c. In Masumoto's model ω_s is linearly proportional to M_s (equation (2)), and therefore the TEC is determined by the ratio M_s/T_c. However, for alloys on the Slater-Pauling curve (e.g., the equiatomic FeNiCo MEA), the relationship between ω_s and M_s follows a quadratic relationship (equation (3)). In order to unify both findings for quantifying the TEC of equiatomic FeNiCo and $Fe_{63}Ni_{32}Co_5$ alloys we define two parameters, the Masumoto parameter M and the Wohlfarth parameter R, according to

$$M = \frac{M_s}{T_c} \quad (5)$$

$$R = \frac{M_s^2}{T_c} \quad (6)$$

where M applies for the $Fe_{63}Ni_{32}Co_5$ alloy, which deviates from the Slater-Pauling curve, and R describes the equiatomic FeNiCo alloy which follows the Slater-Pauling curve. The two parameters, M and R, are employed to distinguish Invar and non-Invar alloys in the following discussion.

4.3. An Invar treasure map guiding the design of novel invar alloys

Based on the above discussion on FeNi binary alloys and FeCoNi MEAs, we include now more of the known Invar alloys and compare those to other metallic materials in an Invar treasure map by considering the relationship among the thermal expansion coefficient, TEC, denoted α in equation (1), the saturation magnetization M_s, and the Curie temperature T_c, as shown in Fig. 8. We use the Masumoto parameter M determined by equation (5) and the Wohlfarth parameter R given by equation (6) to partition the map and indicate ranges of alloys with different TECs. As discussed above, most Invar alloys are ferromagnetically unstable and the actual saturation magnetization is below the value predicted from the Slater-Pauling curve. Therefore, it is better to use the above defined Masumoto parameter M value to describe them. For other alloys (e.g. equiatomic FeCoNi) with normal TEC ($10–20 \times 10^{-6}\,K^{-1}$), most of them follow the Slater-Pauling curve, and hence we employ the Wohlfarth parameter R to quantify them.

We first discuss the parameter M for the map of Invar alloys. In general, from the Invar map in Fig. 8, alloys with lower TECs exhibit larger M values. Since ferromagnetic Invar alloys include disordered solid solutions, amorphous Invar alloys and intermetallic Invar compounds, we discuss them separately in the following.

(1) Disordered solid solution Invar alloys:

These alloys are highlighted in light red in Fig. 8. All of them (e.g. $Fe_{64}Ni_{36}$) have M values larger or equal to 0.42. Particularly, alloys with M values above 0.56 show very low TEC near 0 and even sometimes slight negative values. For instance, the disordered $Fe_{72}Pt_{28}$ alloy has the lowest TEC as well as largest M value compared to other Invar alloys.

(2) Amorphous Invar alloys:

These alloys are highlighted in purple in Fig. 8. All of them have M values larger than 0.6. A typical example group is FeB amorphous alloys in which the TEC increases with increasing B content. $Fe_{79}B_{21}$ has an M value below 0.6 and a TEC above $2 \times 10^{-6}\,K^{-1}$.

(3) Intermetallic Invar compounds:

These compounds are highlighted in light brown in Fig. 8. The trend in the intermetallic Invar compounds is quite different from that in the disordered solid solutions and amorphous alloys. For example, $Er_2Fe_{14}B$

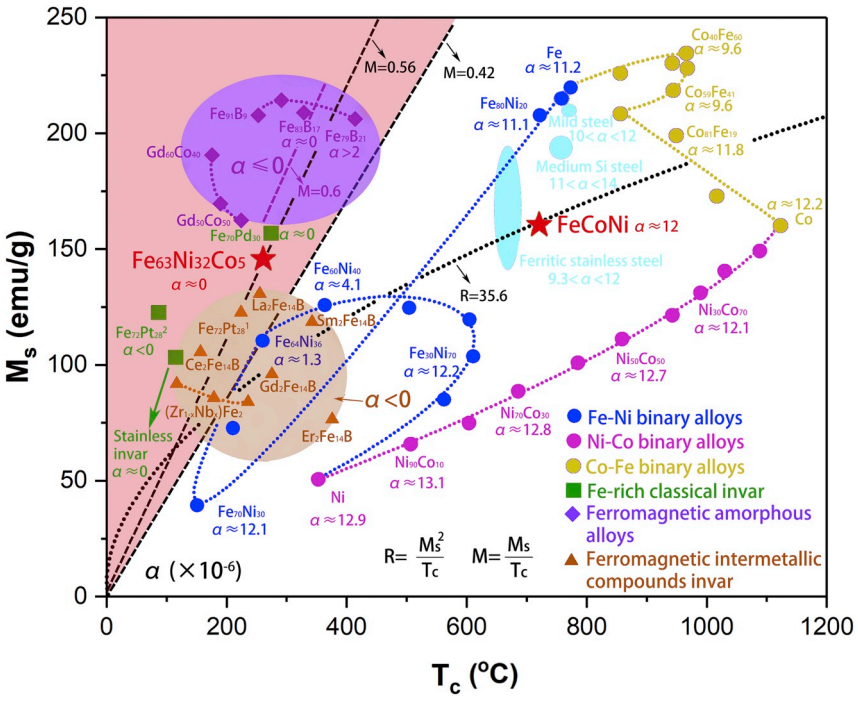

Fig. 8. An Invar treasure map showing several relationships among saturation magnetization (M_s), Curie temperature (T_c) and thermal expansion coefficient (α) of alloy groups and ranges including the non-equiatomic $Fe_{63}Ni_{32}Co_5$ and equiatomic FeNiCo MEAs. The areas for disordered solid solution Invar alloys, amorphous Invar alloys and intermetallic compounds Invar alloys are highlighted in light red, light brown and purple, respectively. Parameters M (Masumoto parameter) and R (Wohlfarth parameter) are applicable for Invar alloys with low α and non-Invar alloys with α of 10–20 $\times 10^{-6} K^{-1}$, respectively. Generally, higher M or R value indicates lower TEC. The disordered solid solution and amorphous Invar alloys have M values larger than 0.42, 0.6 and 0.35, respectively. Data points marked in the map are also listed in Table 2 with corresponding references.

has almost the same M value as pure Ni but it shows negative TEC. This may be caused by the different crystal structure of intermetallic Invar compounds compared to other Invar alloys. The atomic thermally induced vibrations could couple to forces induced by adjacent atomic dipole moments. This could result in the moments of domains in the materials [35,76].

Because most Invar alloys (except for FePt and FePd Invar alloys) are "Slater-Pauling deviation alloys", we can use M to guide our design of new Invar alloys. From 8, all the Invar alloys are in the region in the upper left corner highlighted in light red, light brown and purple. The light red region is for the disordered solid solution which have M values larger than 0.42. The purple region is for amorphous Invar alloys which have M values larger than 0.6. The light brown region is for intermetallic Invar compounds which have M values larger than 0.35. To design new Invar alloys, one should make the M value large enough to reach the numbers above. In fact, this is consistent to Masumoto's rule, i.e. alloys with higher saturation magnetization and lower Curie temperature could have smaller thermal expansion. This rule proposed by Masumoto has already been well used to design $Fe_{63}Ni_{32}Co_5$ super Invar alloy [41] and $Fe_{37}Co_{52}Cr_{11}$ stainless Invar alloy [33].

We next discuss the Wohlfarth parameter R in the map for non-Invar alloys. For alloys with TECs of 10–20 $\times 10^{-6} K^{-1}$, larger R values indicate lower TEC. For instance, the equiatomic FeNiCo alloy has an R value of about 35.6, and alloys with R value larger than 35.6 show TECs lower than that of the equiatomic FeNiCo alloy. Most steels have R values close to that of the equiatomic FeNiCo MEA (i.e. 35.6), and therefore show TECs of around 12 $\times 10^{-6} K^{-1}$. Other typical examples are found for NiCo and CoFe binary alloys: with the increase of the R value from pure Ni to NiCo binary alloys, pure Co, CoFe binary alloys and finally to pure Fe, the R values increase from 6.8 to 60.8 whereas the TECs of the alloys gradually decrease from 12.9 $\times 10^{-6} K^{-1}$ down to 11.2 $\times 10^{-6} K^{-1}$.

Based on the Invar map shown in Fig. 8, it can be understood why the non-equiatomic $Fe_{63}Ni_{32}Co_5$ is an Invar alloy while the equiatomic FeNiCo is not. They have similar values of M_s, but the T_c of the equiatomic FeNiCo is much higher than that of the $Fe_{63}Ni_{32}Co_5$ alloy and therefore the material with equiatomic FeNiCo composition has a much lower M value. As the two alloys have similar Ni content, the difference in TEC values is related to the contents of Fe and Co. Also, it is well-known that the magnetic moment of Ni is much smaller in magnitude compared to that of Fe and Co, thus M_s is here mainly influenced by the Fe and Co contents. On the other hand, the Curie temperature is determined by the average exchange interaction in alloys [58]. According to the Bethe-Slater Curve [77], Co has the largest average exchange interaction among the three elements, and therefore, replacing Co with Fe will decrease the Curie temperature.

It is important to note that the parameter R proposed in the present study shows a much better applicability for describing non-Invar alloys with relatively high TEC compared to the parameter M. The parameter M performs, however, much better as a predictor for the majority of the known Invar alloys in contrast to the parameter R. Overall, both parameters M and R are closely related to the TECs of alloys and can be used to characterize alloys with different TECs. In addition, one should note the limitation of both parameters M and R. This is due to that not only k and A constants in equations (2) and (3) but also other intrinsic material properties such as phase structures may affect the TEC of alloys, especially when the difference of TECs changing from one alloy to another is small.

Our simulations revealed that many important parameters for assessing the Invar performance can be derived from *ab initio* calculations. Among them are the saturation magnetization, the Curie temperatures, and the magnetostriction. In the present work the saturation magnetization for FeCoNi is in excellent agreement with the experimental data. For $Fe_{63}Ni_{32}Co_5$ the saturation magnetization has been slightly overestimated. This could be related to potential antiferromagnetic configurations discussed in Ref. [57] which are, however, not considered in the present calculations. Explicit supercell calculations would be required to further elaborate on this issue and we leave this for future investigations. The mean field predicted Curie temperatures in the present work are also in fair agreement with the experimental data. The derived spontaneous volume magnetostriction ω_s, one of the key parameters in evaluating the Invar performance, correctly predicts a limited Invar behavior of FeCoNi as compared to $Fe_{63}Ni_{32}Co_5$. Based on our findings we can thus conclude that both parameters M and R can be derived from *ab initio* simulations for exploring compositions where required experimental data is lacking.

5. Conclusions

In this work, the microstructure, magnetic properties and thermal expansion behavior of equiatomic FeNiCo and non-equiatomic $Fe_{63}Ni_{32}Co_5$ alloys are studied. Combining Masumoto's model and Wohlfarth's itinerant electron theory, we discussed the relationships among magnetic properties, spontaneous volume magnetostriction and Invar effect in FeCoNi-base MEAs. A comprehensive Invar map was constructed and parameters M and R were proposed to predict the TECs of metallic alloys. The main conclusions are:

(1) Both, non-equiatomic $Fe_{63}Ni_{32}Co_5$ and equiatomic FeNiCo MEAs show single FCC structure with fully recrystallized grains and uniformly distributed elements in the homogenized state.
(2) Both alloys show typical features of soft magnetic materials with high saturation magnetization and low coercivity. The equiatomic FeNiCo alloy has a higher Curie temperature and room temperature saturation magnetization as compared to the non-equiatomic $Fe_{63}Ni_{32}Co_5$ alloy. The equiatomic FeNiCo alloy follows the Slater-Pauling curve while the non-equiatomic $Fe_{63}Ni_{32}Co_5$ alloy deviates from it.
(3) Large values of spontaneous volume magnetization are observed in both alloys. The equiatomic FeNiCo alloy exhibits a peak-type Invar effect with low TECs over a narrow temperature range and the non-equiatomic $Fe_{63}Ni_{32}Co_5$ alloy shows a step-type Invar effect with much lower TEC over a wide temperature range below the Curie temperature. When the alloys are heated above the Curie temperature, i.e., into the paramagnetic state, they have almost the same TEC.
(4) The relationship between spontaneous volume magnetization and saturation magnetization of the equiatomic FeNiCo and non-equiatomic $Fe_{63}Ni_{32}Co_5$ alloys follows different rules. The former fits to the Slater-Pauling curve and shows a quadratic relationship according to Wohlfarth's theory whereas $Fe_{63}Ni_{32}Co_5$ deviates from the Slater-Pauling curve and follows a linear relationship in accord with Masumoto's rule.
(5) Based on Masumoto's model combined with Wohlfarth's theory, we propose to use the parameters M (M_s/T_c) and R (M_s^2/T_c) to predict TECs of metallic alloys. M and R are applicable for Invar alloys with low TECs as well as non-Invar alloys with relatively high TECs.
(6) A treasure map is constructed for Invar alloys compared to other non-Invar alloys. Disordered solid solution and amorphous Invar alloys have M values larger than 0.42 and 0.6, respectively. Most non-Invar alloys with TEC larger than $12 \times 10^{-6}\,K^{-1}$ show R values smaller than 35.6. Replacing Co with Fe in equiatomic FeNiCo alloy will increase the M value, leading to much lower TEC in non-equiatomic $Fe_{63}Ni_{32}Co_5$ alloy.
(7) Based on our discussion, larger M or R values and thus TECs can be achieved by sufficiently low T_c and high ω_s values. By combining available experimental data with computational predictions, the Invar map can be used to discover new Invar HEAs/MEAs in an efficient and theory-guided way.

Acknowledgments

Funding from the Deutsche Forschungsgemeinschaft (SPP 2006) and from NWO/STW (VIDI grant 15707) are gratefully acknowledged. The author (Z. R.) would like to acknowledge the financial support from the China Scholarship Council (CSC). Also acknowledged is the financial support received from the Ministry of Education, Youth and Sports of the Czech Republic under the Project CEITEC 2020, LQ1601 (O.S., M.F.). The kind supports of M. Adamek, B. Breitbach, F. Schlüter, M. Nellessen, K. Angenendt and P. Siegmund at the Max-Planck-Institut für Eisenforschung are gratefully acknowledged.

Appendix A. Supplementary data

Supplementary data to this article can be found online at https://doi.org/10.1016/j.intermet.2019.106520.

Appendix

Table 2
Magnetic properties and thermal expansion coefficient (TEC) of alloys shown in Fig. 8 α indicates the TEC in the vicinity of room temperature. M is the ratio of saturation magnetization M_s and Curie temperature T_c. $Fe_{72}Pt_{28}{}^1$ and $Fe_{72}Pt_{28}{}^2$ indicates ordered and disordered $Fe_{72}Pt_{28}$, respectively.

Alloy (at. %)	T_c	M_s	M	R	α ($\times 10^{-6}$)	Reference
Fe	770	218	0.28	61.7	11.2	[41,78,79]
$Fe_{90}Ni_{10}$	760	215	0.28	60.8	10.8	[41,78,79]
$Fe_{80}Ni_{20}$	720	207	0.29	59.5	11.1	[41,78,79]
$Fe_{70}Ni_{30}$	130	36,5	0.28	10.2	12.1	[41,78,79]
$Fe_{67}Ni_{33}$	210	70	0.33	23.3	3.5	[41,78,79]
$Fe_{64}Ni_{36}$	258	109	0.42	46.1	1.3	[41,78,79]
$Fe_{60}Ni_{40}$	360	125	0.35	43.4	4.1	[41,78,79]
$Fe_{50}Ni_{50}$	505	125	0.25	30.9	9.7	[41,78,79]
$Fe_{40}Ni_{60}$	605	118	0.20	23.0	11.3	[41,78,79]
$Fe_{30}Ni_{70}$	610	103	0.17	17.4	12.2	[41,78,79]
$Fe_{20}Ni_{80}$	560	85	0.15	12.9	12.8	[41,78,79]
Ni	354	49	0.14	6.8	12.89	[41,78,79]
$Ni_{90}Co_{10}$	505	66	0.13	8.6	13.1	[41,78,79]
$Ni_{80}Co_{20}$	605	75	0.12	9.3	12.8	[41,78,79]
$Ni_{70}Co_{30}$	690	89	0.13	11.5	12.8	[41,78,79]
$Ni_{60}Co_{40}$	790	101	0.13	12.9	12.6	[41,78,79]
$Ni_{50}Co_{50}$	860	112	0.13	14.6	12.7	[41,78,79]
$Ni_{40}Co_{60}$	940	122	0.13	15.8	12.4	[41,78,79]
$Ni_{30}Co_{70}$	990	132	0.13	17.6	12.1	[41,78,79]
$Ni_{20}Co_{80}$	1030	141	0.14	19.3	12.8	[41,78,79]
$Ni_{10}Co_{90}$	1090	149	0.14	20.4	12.6	[41,78,79]
Co	1127	160	0.14	22.7	12.2	[41,78,79]
$Co_{90}Fe_{10}$	1027	173	0.17	29.1	11.7	[41,78,79]
$Co_{81}Fe_{19}$	947	189	0.20	37.7	11.8	[41,78,79]
$Co_{69}Fe_{31}$	857	209	0.24	51.0	10	[41,78,79]

(*continued on next page*)

Table 2 (*continued*)

Alloy (at. %)	T_c	M_s	M	R	α ($\times 10^{-6}$)	Reference
$Co_{59}Fe_{41}$	946	219	0.23	50.7	9.6	[41,78,79]
$Co_{49}Fe_{51}$	964	229	0.24	54.4	9.3	[41,78,79]
$Co_{40}Fe_{60}$	964	235	0.24	57.3	9.6	[41,78,79]
$Co_{30}Fe_{70}$	964	235	0.24	57.3	9.7	[41,78,79]
$Co_{20}Fe_{80}$	946	229	0.24	55.4	10.1	[41,78,79]
$Co_{10}Fe_{90}$	857	225	0.26	59.1	11.2	[41,78,79]
$Fe_{72}Pt_{28}$(ordered)	227	123	0.54	66.6	< 0	[80]
$Fe_{72}Pt_{28}$(disordered)	87	123	1.41	173.9	< 0	[80]
$Fe_{37}Co_{52}Cr_{11}$	117	102	0.87	88.9	0	[81,82]
$Fe_{33.4}Co_{33.3}Ni_{33.3}$	720	160	0.22	35.6	12	Current work
$Fe_{63}Ni_{32}Co_5$	260	145	0.56	80.9	0	Current work
$Fe_{70}Pd_{30}$	273	157	0.58	90.3	0	[34]
$Fe_{91}B_9$	250	206	0.82	169.7	< 0	[25]
$Fe_{85}B_{15}$	300	213	0.71	151.2	< 0	[25]
$Fe_{83}B_{17}$	320	210	0.66	137.8	≈ 0	[25]
$Fe_{79}B_{21}$	410	206	0.50	103.5	> 2	[25]
$Gd_{60}Co_{40}$	170	190	1.12	212.4	≈ 0	[30]
$Gd_{55}Co_{45}$	190	170	0.89	152.1	≈ 0	[30]
$Gd_{50}Co_{50}$	230	160	0.70	111.3	≈ 0	[30]
$(Zr_{0.9}Nb_{0.1})Fe_2$	237	84	0.35	29.8	< 0	[35]
$(Zr_{0.8}Nb_{0.2})Fe_2$	177	86	0.49	41.8	< 0	[35]
$(Zr_{0.7}Nb_{0.3})Fe_2$	117	92	0.79	72.3	< 0	[35]
$La_2Fe_{14}B$	257	130	0.51	65.8	< 0	[26]
$Ce_2Fe_{14}B$	152	105	0.69	72.5	< 0	[26]
$Er_2Fe_{14}B$	277	96	0.35	33.3	< 0	[26]
$Sm_2Fe_{14}B$	343	120	0.35	42.0	< 0	[26]
$Gd_2Fe_{14}B$	377	77	0.20	15.7	< 0	[26]
Ferritic stainless steel (10.7–27 at.% Cr)	660–650	185–130	0.2–0.28	26–57	9.3–12	[59,83,84]
Ductile medium-silicon cast iron (4.5 at. % Si)	750–760	185–195	0.25–0.26	45.6–50	11.0–14	[59,83,84]
Mild steel	770	212	0.28	58.4	10 12	[59,83,84]

References

[1] J.W. Yeh, S.K. Chen, S.J. Lin, J.Y. Gan, T.S. Chin, T.T. Shun, C.H. Tsau, S.Y. Chang, Nanostructured high-entropy alloys with multiple principal elements: novel alloy design concepts and outcomes, Adv. Eng. Mater. 6 (5) (2004) 299–303.

[2] B. Cantor, I. Chang, P. Knight, A. Vincent, Microstructural development in equiatomic multicomponent alloys, Mater. Sci. Eng. A 375 (2004) 213–218.

[3] Y. Zhang, T.T. Zuo, Z. Tang, M.C. Gao, K.A. Dahmen, P.K. Liaw, Z.P. Lu, Microstructures and properties of high-entropy alloys, Prog. Mater. Sci. 61 (2014) 1–93.

[4] Y. Zhang, Y.J. Zhou, J.P. Lin, G.L. Chen, P.K. Liaw, Solid-solution phase formation rules for multi-component alloys, Adv. Eng. Mater. 10 (6) (2008) 534–538.

[5] Y. Jien-Wei, Recent progress in high entropy alloys, Ann. Chim. Sci. Mat 31 (6) (2006) 633–648.

[6] B. Gludovatz, A. Hohenwarter, D. Catoor, E.H. Chang, E.P. George, R.O. Ritchie, A fracture-resistant high-entropy alloy for cryogenic applications, Science 345 (6201) (2014) 1153–1158.

[7] P. Koželj, S. Vrtnik, A. Jelen, S. Jazbec, Z. Jagličić, S. Maiti, M. Feuerbacher, W. Steurer, J. Dolinšek, Discovery of a superconducting high-entropy alloy, Phys. Rev. Lett. 113 (10) (2014) 107001.

[8] Y. Yuan, Y. Wu, X. Tong, H. Zhang, H. Wang, X. Liu, L. Ma, H. Suo, Z. Lu, Rare-earth high-entropy alloys with giant magnetocaloric effect, Acta Mater. 125 (2017) 481–489.

[9] B. Gludovatz, A. Hohenwarter, K.V. Thurston, H. Bei, Z. Wu, E.P. George, R.O. Ritchie, Exceptional damage-tolerance of a medium-entropy alloy CrCoNi at cryogenic temperatures, Nat. Commun. 7 (2016) 10602.

[10] Z. Li, C.C. Tasan, H. Springer, B. Gault, D. Raabe, Interstitial atoms enable joint twinning and transformation induced plasticity in strong and ductile high-entropy alloys, Sci. Rep. 7 (2017) 40704.

[11] Z. Li, D. Raabe, Strong and ductile non-equiatomic high-entropy alloys: design, processing, microstructure, and mechanical properties, JOM 69 (11) (2017) 2099–2106.

[12] Z. Li, F. Körmann, B. Grabowski, J. Neugebauer, D. Raabe, *Ab initio* assisted design of quinary dual-phase high-entropy alloys with transformation-induced plasticity, Acta Mater. 136 (2017) 262–270.

[13] G. Laplanche, A. Kostka, C. Reinhart, J. Hunfeld, G. Eggeler, E. George, Reasons for the superior mechanical properties of medium-entropy CrCoNi compared to high-entropy CrMnFeCoNi, Acta Mater. 128 (2017) 292–303.

[14] J. Miao, C. Slone, T. Smith, C. Niu, H. Bei, M. Ghazisaeidi, G. Pharr, M.J. Mills, The evolution of the deformation substructure in a Ni-Co-Cr equiatomic solid solution alloy, Acta Mater. 132 (2017) 35–48.

[15] S. Yoshida, T. Bhattacharjee, Y. Bai, N. Tsuji, Friction stress and Hall-Petch relationship in CoCrNi equi-atomic medium entropy alloy processed by severe plastic deformation and subsequent annealing, Scripta Mater. 134 (2017) 33–36.

[16] Z. Zhang, H. Sheng, Z. Wang, B. Gludovatz, Z. Zhang, E.P. George, Q. Yu, S.X. Mao, R.O. Ritchie, Dislocation mechanisms and 3D twin architectures generate exceptional strength-ductility-toughness combination in CrCoNi medium-entropy alloy, Nat. Commun. 8 (2017) 14390.

[17] Y. Zhao, T. Yang, Y. Tong, J. Wang, J. Luan, Z. Jiao, D. Chen, Y. Yang, A. Hu, C. Liu, Heterogeneous precipitation behavior and stacking-fault-mediated deformation in a CoCrNi-based medium-entropy alloy, Acta Mater. 138 (2017) 72–82.

[18] D. Miracle, O. Senkov, A critical review of high entropy alloys and related concepts, Acta Mater. 122 (2017) 448–511.

[19] Z. Zhang, M. Mao, J. Wang, B. Gludovatz, Z. Zhang, S.X. Mao, E.P. George, Q. Yu, R.O. Ritchie, Nanoscale origins of the damage tolerance of the high-entropy alloy CrMnFeCoNi, Nat. Commun. 6 (2015) 10143.

[20] B. Gludovatz, E.P. George, R.O. Ritchie, Processing, Microstructure and mechanical properties of the CrMnFeCoNi high-entropy alloy, JOM 67 (10) (2015) 2262–2270.

[21] M. Laktionova, E. Tabchnikova, Z. Tang, P. Liaw, Mechanical properties of the high-entropy alloy $Ag_{0.5}$CoCrCuFeNi at temperatures of 4.2-300 K, Low Temp. Phys. 39 (7) (2013) 630–632.

[22] O. Senkov, G. Wilks, J. Scott, D. Miracle, Mechanical properties of $Nb_{25}Mo_{25}Ta_{25}W_{25}$ and $V_{20}Nb_{20}Mo_{20}Ta_{20}W_{20}$ refractory high entropy alloys, Intermetallics 19 (5) (2011) 698–706.

[23] O. Schneeweiss, M. Friák, M. Dudová, D. Holec, M. Šob, D. Kriegner, V. Holý, P. Beran, E.P. George, J. Neugebauer, Magnetic properties of the CrMnFeCoNi high-entropy alloy, Phys. Rev. B 96 (1) (2017) 014437.

[24] H. Saito, Physics and Applications of Invar Alloys, Maruzen, 1978.

[25] K. Fukamichi, M. Kikuchi, S. Arakawa, T. Masumoto, Invar-type new ferromagnetic amorphous Fe-B alloys, Solid State Commun. 23 (12) (1977) 955–958.

[26] K. Buschow, Invar effect in $R_2Fe_{14}B$ compounds (R-La, Ce, Nd, Sm, Gd, Er), J. Less Common Met. 118 (2) (1986) 349–353.

[27] P. Gorria, D. Martínez-Blanco, J.A. Blanco, A. Hernando, J.S. Garitaonandia, L.F. Barquín, J. Campo, R.I. Smith, Invar effect in fcc-FeCu solid solutions, Phys. Rev. B 69 (21) (2004) 214421.

[28] Q. Hu, X.-R. Zeng, M.-W. Fu, Invar effects of $(Fe_{71.2}B_{24}Y_{4.8})_{96}Nb_4$ alloy in different structural states, Appl. Phys. Lett. 97 (22) (2010) 221907.

[29] Q. Hu, J. Wang, Y. Yan, S. Guo, S. Chen, D. Lu, J. Zou, X. Zeng, Invar effect of Fe-based bulk metallic glasses, Intermetallics 93 (2018) 318–322.

[30] K. Fukamichi, M. Kikuchi, T. Masumoto, M. Matsuura, Magnetic properties and Invar effects of amorphous Gd-Co ribbons, Phys. Lett. 73 (5–6) (1979) 436–438.

[31] L. Graf, A. Kussmann, Zustandsdiagramm und magnetische Eigenschaften von Platin-Eisen-Legierungen, Z. Phys. 36 (1935) 544–551.

[32] P. Hidnert, R.K. Kirby, Thermal expansion and phase transformations of low-expanding cobalt-iron-chromium alloys, J. Res. Nat. Bur. Stand 55 (29) (1955) 37.

[33] K. Honda, A new alloy,'Stainless-Invar', Nature 131 (3312) (1933) 587.

[34] A. Kussmann, K. Jessen, Invar-behaviour and magnetic moments of gamma-phase of iron-palladium alloys, J. Phys. Soc. Jpn. 17 (1962) 136.

[35] M. Shiga, Y. Nakamura, Magnetovolume effects and invar characters of $(Zr_{1-x}Nbx)Fe_2$, J. Phys. Soc. Jpn. 47 (5) (1979) 1446–1451.

[36] A. Lawson, J. Roberts, B. Martinez, J. Richardson, Invar effect in Pu-Ga alloys,

Philos. Mag. B 82 (18) (2002) 1837–1845.
[37] C.É. Guillaume, Recherches sur les aciers au nickel. Dilatations aux temperatures elevees; resistance electrique, C. R. Acad. Sci. 125 (235) (1897) 18.
[38] F. Liot, I. Abrikosov, Local magnetovolume effects in $Fe_{65}Ni_{35}$ alloys, Phys. Rev. B 79 (1) (2009) 014202.
[39] T. Yokoyama, K. Eguchi, Anisotropic thermal expansion and cooperative Invar and anti-Invar effects in Mn alloys, Phys. Rev. Lett. 110 (7) (2013) 075901.
[40] J. Monroe, D. Gehring, I. Karaman, R. Arroyave, D.W. Brown, B. Clausen, Tailored thermal expansion alloys, Acta Mater. 102 (2016) 333–341.
[41] H. Masumoto, On the Thermal Expansion of the Alloys of Iron, Nickel, and Cobalt and the Cause of the Small Expansibility of Alloys of the Invar Type vol. 20, Science Reports of the Tohoku Imperial University, 1931, pp. 101–123.
[42] R. Weiss, The origin of the Invar effect, Proc. Phys. Soc. 82 (2) (1963) 281.
[43] E. Wohlfarth, Contributions to the invar problem II, Phys. Lett. 28 (8) (1969) 569–570.
[44] E. Wohlfarth, Forced magnetostriction in the band model of magnetism, J. Phys. C Solid State Phys. 2 (1) (1969) 68.
[45] L. Vitos, H.L. Skriver, B. Johansson, J. Kollár, Application of the exact muffin-tin orbitals theory: the spherical cell approximation, Comput. Mater. Sci. 18 (1) (2000) 24–38.
[46] L. Vitos, J. Kollár, H.L. Skriver, Full charge-density calculation of the surface energy of metals, Phys. Rev. B 49 (23) (1994) 16694.
[47] L. Vitos, J. Kollár, H.L. Skriver, Full charge-density scheme with a kinetic-energy correction: application to ground-state properties of the 4d metals, Phys. Rev. B 55 (20) (1997) 13521.
[48] P. Soven, Coherent-potential model of substitutional disordered alloys, Phys. Rev. 156 (3) (1967) 809.
[49] B. Gyorffy, Coherent-potential approximation for a nonoverlapping-muffin-tin-potential model of random substitutional alloys, Phys. Rev. B 5 (6) (1972) 2382.
[50] J.P. Perdew, K. Burke, M. Ernzerhof, Generalized gradient approximation made simple, Phys. Rev. Lett. 77 (18) (1996) 3865.
[51] L. Vitos, Computational Quantum Mechanics for Materials Engineers: the EMTO Method and Applications, Springer Science & Business Media, 2007.
[52] J. Staunton, B. Gyorffy, A. Pindor, G. Stocks, H. Winter, The "disordered local moment" picture of itinerant magnetism at finite temperatures, J. Magn. Magn. Mater. 45 (1) (1984) 15–22.
[53] B. Gyorffy, A. Pindor, J. Staunton, G. Stocks, H. Winter, A first-principles theory of ferromagnetic phase transitions in metals, J. Phys. F Met. Phys. 15 (6) (1985) 1337.
[54] F. Körmann, D. Ma, D.D. Belyea, M.S. Lucas, C.W. Miller, B. Grabowski, M.H. Sluiter, "Treasure maps" for magnetic high-entropy-alloys from theory and experiment, Appl. Phys. Lett. 107 (14) (2015) 142404.
[55] Y. Ikeda, B. Grabowski, F. Körmann, Ab initio phase stabilities and mechanical properties of multicomponent alloys: a comprehensive review for high entropy alloys and compositionally complex alloys, Mater. Char. 147 (2018) 464–511.
[56] H. Song, F. Tian, Q.-M. Hu, L. Vitos, Y. Wang, J. Shen, N. Chen, Local lattice distortion in high-entropy alloys, Phys. Rev. Mater. 1 (2) (2017) 023404.
[57] A.V. Ruban, S. Khmelevskyi, P. Mohn, B. Johansson, Magnetic state, magnetovolume effects, and atomic order in $Fe_{65}Ni_{35}$Invar alloy: a first principles study, Phys. Rev. B 76 (1) (2007) 014420.
[58] C.R. Clayton, Materials Science and Engineering: an Introduction: by WD Callister Jr. published by Wiley, Chichester, West Sussex, 1985, p. 602 Elsevier, 1987.
[59] R.M. Bozorth, Richard M. Bozorth (Ed.), Ferromagnetism, Ferromagnetism, Wiley-VCH, 0-7803-1032-2, August 1993, p. 992 (1993) 992.
[60] S. Jen, H. Chiang, C. Chung, M. Kao, Magnetic properties of Co–Fe–Ni films, J. Magn. Magn. Mater. 236 (3) (2001) 312–319.
[61] T. Mashimo, X. Huang, X. Fan, K. Koyama, M. Motokawa, Slater-Pauling curve of Fe-Cu solid solution alloys, Phys. Rev. B 66 (13) (2002) 132407.
[62] M. Shiga, Invar alloys, Curr. Opin. Solid State Mater. Sci. 1 (3) (1996) 340–348.
[63] V. Crisan, P. Entel, H. Ebert, H. Akai, D.D. Johnson, J. Staunton, Magnetochemical origin for Invar anomalies in iron-nickel alloys, Phys. Rev. B 66 (1) (2002) 014416.
[64] S. Khmelevskyi, P. Mohn, Magnetostriction in Fe-based alloys and the origin of the Invar anomaly, Phys. Rev. B 69 (14) (2004) 140404.
[65] A.V. Ruban, First-principles modeling of the Invar effect in $Fe_{65}Ni_{35}$ by the spin-wave method, Phys. Rev. B 95 (17) (2017) 174432.
[66] Y. Ikeda, F. Körmann, B. Dutta, A. Carreras, A. Seko, J. Neugebauer, I. Tanaka, Temperature-dependent phonon spectra of magnetic random solid solutions, Npj Comput. Mater. 4 (1) (2018) 7.
[67] I. Abrikosov, O. Eriksson, P. Söderlind, H.L. Skriver, B. Johansson, Theoretical aspects of the Fe_cNi_{1-c} Invar alloy, Phys. Rev. B 51 (2) (1995) 1058.
[68] E. Smirnova, I. Abrikosov, B. Johansson, Y.K. Vekilov, A. Baranov, V. Stepanyuk, W. Hergert, P. Dederichs, Calculated magnetic properties of an $Fe_{1-x}Ni_x$ monolayer on Cu (001), Phys. Rev. B 59 (22) (1999) 14417.
[69] M. van Schilfgaarde, I. Abrikosov, B. Johansson, Origin of the Invar effect in iron–nickel alloys, Nature 400 (6739) (1999) 46.
[70] L. Dubrovinsky, N. Dubrovinskaia, I.A. Abrikosov, M. Vennström, F. Westman, S. Carlson, M. van Schilfgaarde, B. Johansson, Pressure-induced Invar effect in Fe-Ni alloys, Phys. Rev. Lett. 86 (21) (2001) 4851.
[71] F. Liot, S. Simak, I. Abrikosov, Static ionic displacements in Fe–Ni alloys from first principles, J. Appl. Phys. 99 (8) (2006) 08P906.
[72] K. Lagarec, D. Rancourt, S. Bose, B. Sanyal, R. Dunlap, Observation of a composition-controlled high-moment/low-moment transition in the face centered cubic Fe–Ni system: invar effect is an expansion, not a contraction, J. Magn. Magn. Mater. 236 (1–2) (2001) 107–130.
[73] D. Lencer, M. Salinga, B. Grabowski, T. Hickel, J. Neugebauer, M. Wuttig, A map for phase-change materials, Nature Mater 7 (12) (2008) 972.
[74] T. Nakajima, Effect of pressure on the Curie temperature in Invar-type iron-platinum alloys as a phase transition of the second kind, J. Phys. Soc. Jpn. 19 (4) (1964) 520–529.
[75] H. Masumoto, S. Sawaya, M. Kikuchi, Thermal expansion coefficient, temperature coefficient of Young's Modulus and equilibrium diagram of ferromagnetic Cobalt-Manganese alloys, Trans. Jpn. Inst. Met. 11 (3) (1970) 171–175.
[76] S. Sinnema, R. Radwanski, J. Franse, D. De Mooij, K. Buschow, Magnetic properties of ternary rare-earth compounds of the type $R_2Fe_{14}B$, J. Magn. Magn. Mater. 44 (3) (1984) 333–341.
[77] S. Chikazumi, C.D. Graham, Physics of Ferromagnetism 2e, Oxford University Press on Demand, 2009.
[78] W.S. McCain, R.M. Maringer, Mechanical and Physical Properties of Invar and Invar-type Alloys, Battelle Memorial Inst Columbus Oh Defense Metals Information Center, 1965.
[79] F. Pfeifer, C. Radeloff, Soft magnetic Ni-Fe and Co-Fe alloys-some physical and metallurgical aspects, J. Magn. Magn. Mater. 19 (1–3) (1980) 190–207.
[80] K. Sumiyama, M. Shiga, Y. Kobayahsi, K. Nishi, Y. Nakamura, Strong ferromagnetism in Invar type Fe-Pt alloys, J. Phys. F Met. Phys. 8 (6) (1978) 1281.
[81] H. Fujimori, H. Saitô, On the magnetic and electric properties of $(Fe_{1-x}Co_x)_{0.89}Cr_{0.11}$ alloys, Trans. Jpn. Inst. Met. 11 (1) (1970) 72–76.
[82] Y. Nakamura, The Invar problem, IEEE Trans. Magn. 12 (4) (1976) 278–291.
[83] A.M. Handbook, Properties and Selection: Stainless Steels, Tool Materials and Special-Purpose Metals vol. 3, Am. Soc. Met., Met. Park, OH, 1985, pp. 893–899.
[84] A.S.f. Metals, Metals Handbook. Vol. 1. Properties and Selection Irons and Steels, ASM, 1978.